Supporting Information

Structure evolution of $NiMn_2O_4$-based materials induced by atmosphere and its impact on dry reforming of methane activity

Jun Duan,[a] Xueying Zheng,[a] Shiying Fan,[a] Shaomin Liu,[b] and Xinyong Li*[a]

[a]*State Key Laboratory of Fine Chemicals, Key Laboratory of Industrial Ecology and Environmental Engineering (MOE), School of Environmental Science and Technology, Dalian University of Technology, Dalian 116024, PR China*

[b]*Dongguan Key Laboratory of Intelligent Equipment and Smart Industry, School of Engineering, Great Bay University, Dongguan 523000, China.*

Corresponding author:

Email address: xyli@dlut.edu.cn (X. Li);

1. Experiment

1.1. Chemicals and materials

The reagents used include nickel nitrate hexahydrate ($Ni(NO_3)_2 \cdot 4H_2O$, 98.0%), manganese nitrate tetrahydrate ($Mn(NO_3)_2 \cdot 6H_2O$, 98.0%), glycerol (≥ 99.0%, 1.250-1.264 g mL^{-1} at 20 ℃), isopropanol (≥ 99.7%, 0.784-0.786 g mL^{-1} at 20 ℃), and ethanol (≥ 99.7%, 0.789-0.791 mL^{-1} at 20 ℃).

1.2. Materials synthesis

A homogeneous solution was prepared by dissolving 0.25 mmol of $Ni(NO_3)_2 \cdot 4H_2O$ and 0.5 mmol of $Mn(NO_3)_2 \cdot 6H_2O$ in 80 mL of isopropanol containing 16 mL of glycerol under continuous stirring. After magnetically stirring at room temperature for 60 min, the well-dispersed solution was transferred into a 100 mL Teflon-lined autoclave and hydrothermally treated at 180 ℃ for 6 h. The resulting precipitate was collected by centrifugation, washed with ethanol, and vacuum-dried overnight. The as-obtained precursor was then annealed in a tube furnace under a gas flow of 50 mL min^{-1}. After purging at room temperature for 30 min, the temperature was raised to 400 ℃ at a heating rate of 1 ℃ min^{-1} and held for 2 h before cooling to ambient conditions. Four calcination atmospheres were employed: air, argon (Ar), and hydrogen (H_2), yielding the $NiMn_2O_4$ materials (NMO) denoted as NMO-Air, NMO-Ar, and NMO-H_2. An additional sample, NMO-Air+H_2, was synthesized by first calcining the precursor in air (1 ℃ min^{-1} to 400 ℃, 2 h), followed by reduction under H_2 using the same temperature program as the dry reforming of methane (DRM) activity test (10 ℃ min^{-1} to 400 ℃, 2 h).

1.3. Characterizations

The X-ray diffraction (XRD) patterns were recorded by using a BRUKER D8 ADVANCE equipped with Cu Kα radiation. Fourier transform infrared reflection (FTIR) spectra were collected on a BRUKER VERTEX 70 FTIR spectrometer. The Raman spectra were performed via a Renishaw inVia Qontor. The scanning electron microscopy (SEM) and transmission electron microscopy (TEM) images were measured on SU5000 ultrahigh resolution field emission scanning electron microscopy and FEI Tecnai G2F30 STWIN, respectively. Concurrently, the elemental composition of the catalyst was further examined using X-ray energy dispersive spectroscopy (EDS). N_2 adsorption-desorption isotherms were studied on a Quantachrome equipment (NOVA 4200e) instrument to analyze the surface area and pore size distribution. X-ray photoelectron spectroscopy (XPS) was recorded in a Thermos K-Alpha+ spectrometer. Low-temperature electron paramagnetic resonance (EPR) was conducted by a Bruker A300 Electron Paramagnetic Resonance Spectrometer from Germany.

In-situ temperature-programmed (TP) experiments were conducted using a chemisorption analyzer (manufactured by Anton Paar, America). Here, 50 mg catalysts were paced into a U-shaped quartz tube for chemisorption tests. For hydrogen temperature-programmed reduction experiments (H_2-TPR), the apparatus was equipped with a cold trap containing a gel mixture of isopropyl alcohol and liquid nitrogen. Initially, the samples were pretreated at 200 °C in a high-purity helium atmosphere (30 mL min^{-1}) for 30 min and cooled down to room temperature naturally.

Then, the temperature was gradually increased to 800 °C at a heating rate of 10 °C min^{-1} in a 10% H_2/Ar mixture atmosphere (30 mL/min). For a series of temperature-programmed desorption experiments (NH_3-TPD/CO_2-TPD/O_2-TPD), the samples were pretreated at 200 °C in a high-purity helium atmosphere (30 mL min^{-1}) for 30 min. After cooling down to room temperature naturally, the samples were exposed to the 10% mixture (NH_3/Ar, CO_2/Ar, O_2/Ar) atmosphere (30 mL min^{-1}) for 1 h until achieving adsorption saturation. Then, the samples were purged in a helium atmosphere at room temperature at a flow rate of 30 mL min^{-1} for 30 min, followed by heating from room temperature to 900 °C at a heating rate of 10 °C min^{-1}.

1.4. DRM Reaction

The activity tests of DRM were carried out continuously in a fix bed system. In each reaction, 50 mg of screened 40-60 mesh samples were placed in the quartz tube with quartz cotton placed at both ends to prevent leakage. The quartz tube was installed in the YDL type electric heating furnace of the *in-situ* evaluation system. In a typical DRM reaction, the catalyst was pretreated in an Ar atmosphere (30 mL min^{-1}) by heating to 300 °C at a heating rate of 10 °C min^{-1} for 30 min. Then, the mixture gas of CH_4/CO_2/Ar=1/1/3 (30 mL min^{-1}) was introduced and heated to 700 °C at a heating rate of 10 °C min^{-1} and maintained every 50 °C for 60 min for reaction and data collection. To detecting the change of gas composition, the tail gas was continuously introduced into a gas chromatograph (GC7890A, manufactured by Agilent Technologies Co., LTD.). The GC apparatus was equipped with TCD detector, PQ and 5A equipped as chromatographic columns, with Ar as carrier gas. The DRM

performances were studied based on CH_4 and CO_2 conversion rates (χ_{CH_4},χ_{CO_2}), and H_2/CO ratio. The produced syngas productivity was calculated by ideal gas equation.

$$\chi_{CH_4}(\%) = (A_{CH_4}{}^{in} - A_{CH_4}{}^{out}) \Big/ A_{CH_4}{}^{in} \times 100\% \#(1)$$

$$\chi_{CO_2}(\%) = (A_{CO_2}{}^{in} - A_{CO_2}{}^{out}) \Big/ A_{CO_2}{}^{in} \times 100\% \#(2)$$

$$H_2/CO = V_{H_2}/V_{CO} \#(3)$$

Where $A_{CH_4}{}^{in}$, $A_{CH_4}{}^{out}$, $A_{CO_2}{}^{in}$, $A_{CO_2}{}^{out}$, represent the integral area of inward and outward of CH_4, CO_2; V_{H_2}, V_{CO}, refer to the volume of H_2 and CO detected by GC, respectively.

2. Figures and Tables

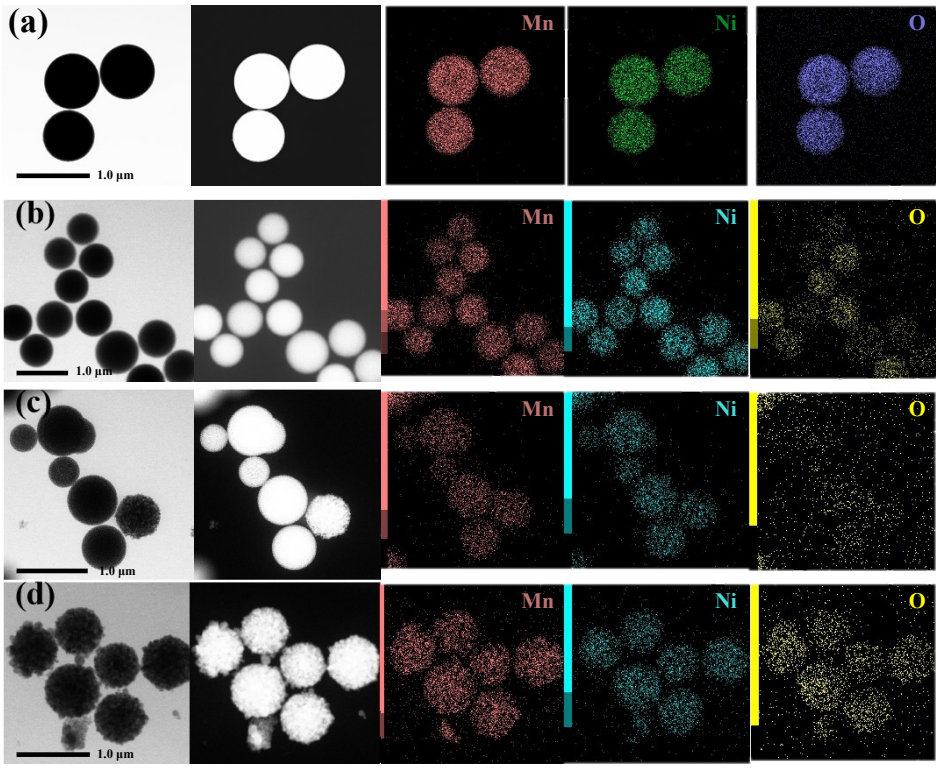

Fig. S1 TEM images and EDS mapping of catalysts after calcination in different atmospheres: (a) NMO-Air, (b) NMO-Ar, (c) NMO-Air+H_2, and (d) NMO-H_2.

As the process proceeds, internal O atoms must diffuse through the already reduced outer layers to reach the surface, where they were subsequently reduced by H_2 and escaped. However, this diffusion pathway was protracted and intricate, likely hindered by lattice defects or grain boundaries, ultimately impairing uniform O migration to the surface. In contrast, direct H_2 reduction of the precursor enabled simultaneous reduction of Ni and Mn oxides, allowing more orderly atomic diffusion and facilitating homogeneous Ni/MnO formation.

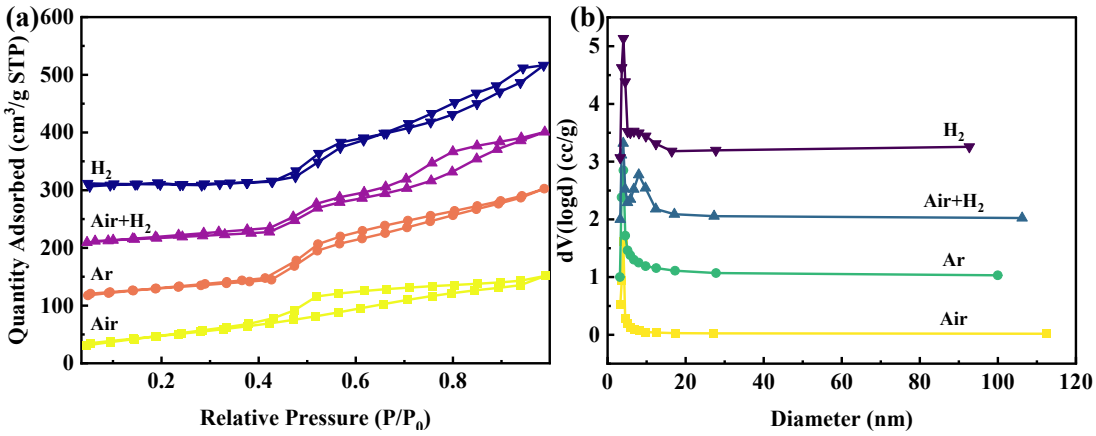

Fig. S2 (a) The N_2 adsorption-desorption isotherms and (b) pore diameter distribution curves.

Table. S1 Structural properties and integrated peak area of the total amount of H_2 consumption, CO_2 desorption and NH_3 desorption.

Sample	BET surface area (m^2 g^{-1})	Pore size (nm)	Pore volume (cm^3 g^{-1})	H_2 consumption peak area (a.u.)	CO_2 desorption peak area (a.u.)	NH_3 desorption peak area (a.u.)
NMO-Air	178.54	4.026	0.220	17266	5526	6098
NMO-Ar	116.82	4.060	0.386	33502	4688	7449
NMO-Air+H_2	71.595	4.015	0.391	4383	5268	5609
NMO-H_2	32.796	4.052	0.598	2792	1826	1213

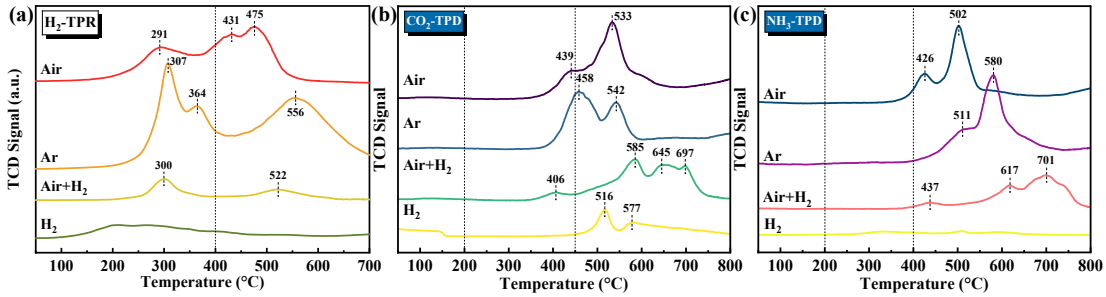

123

124 **Fig. S3** (a) H_2-TPR, (b) CO_2-TPD, and (c) NH_3-TPD of catalysts after calcination in

125 different atmospheres.

126

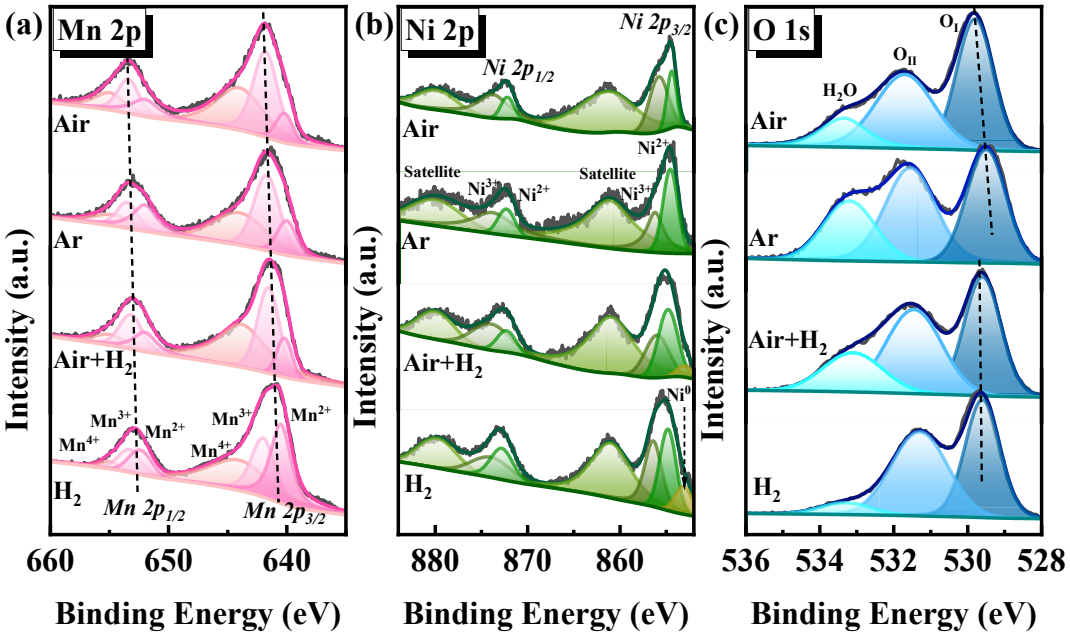

127

128 **Fig. S4** XPS spectra of as-prepared catalysts: (a) Mn 2p, (b) Ni 2p, and (c) O 1 s.

129

Table. S2 The XPS results of the samples

Sample	O species		
	H_2O ratio	O_{II} ratio	O_I ratio
NMO-Air	0.12	0.39	0.49
NMO-Ar	0.29	0.35	0.36
NMO-Air+H_2	0.16	0.46	0.38
NMO-H_2	0.02	0.50	0.48

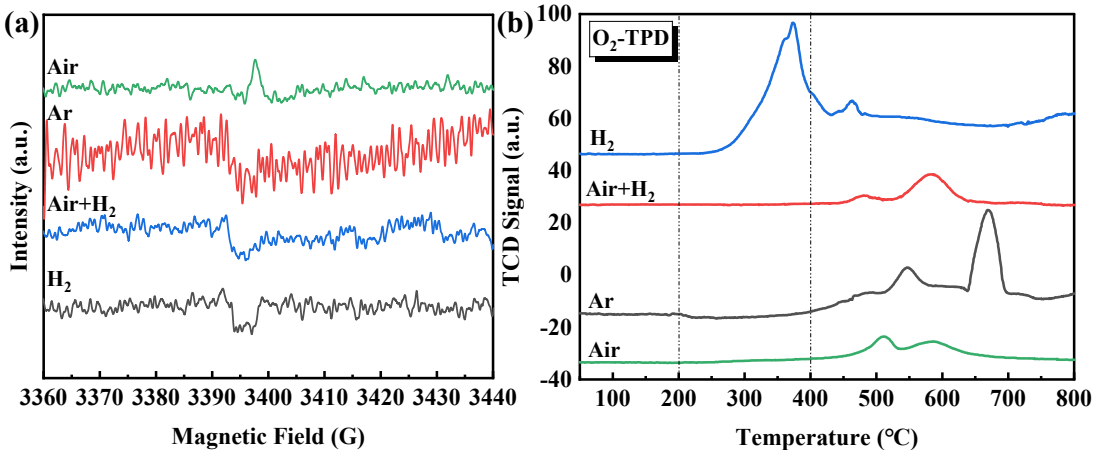

132

133 **Fig. S5** The (a) low-temperature EPR and (b) O_2-TPD of materials.

134

135 The O_2-TPD profiles of all catalysts could be divided into three characteristic

136 temperature regions: < 200 °C, 200-400 °C, and > 400 °C, corresponding to the

137 desorption of chemisorbed oxygen species desorbed from surfaces,[1] surface, and bulk

138 lattice oxygen species,[2] respectively. All samples showed negligible desorption below

139 200 °C.

140

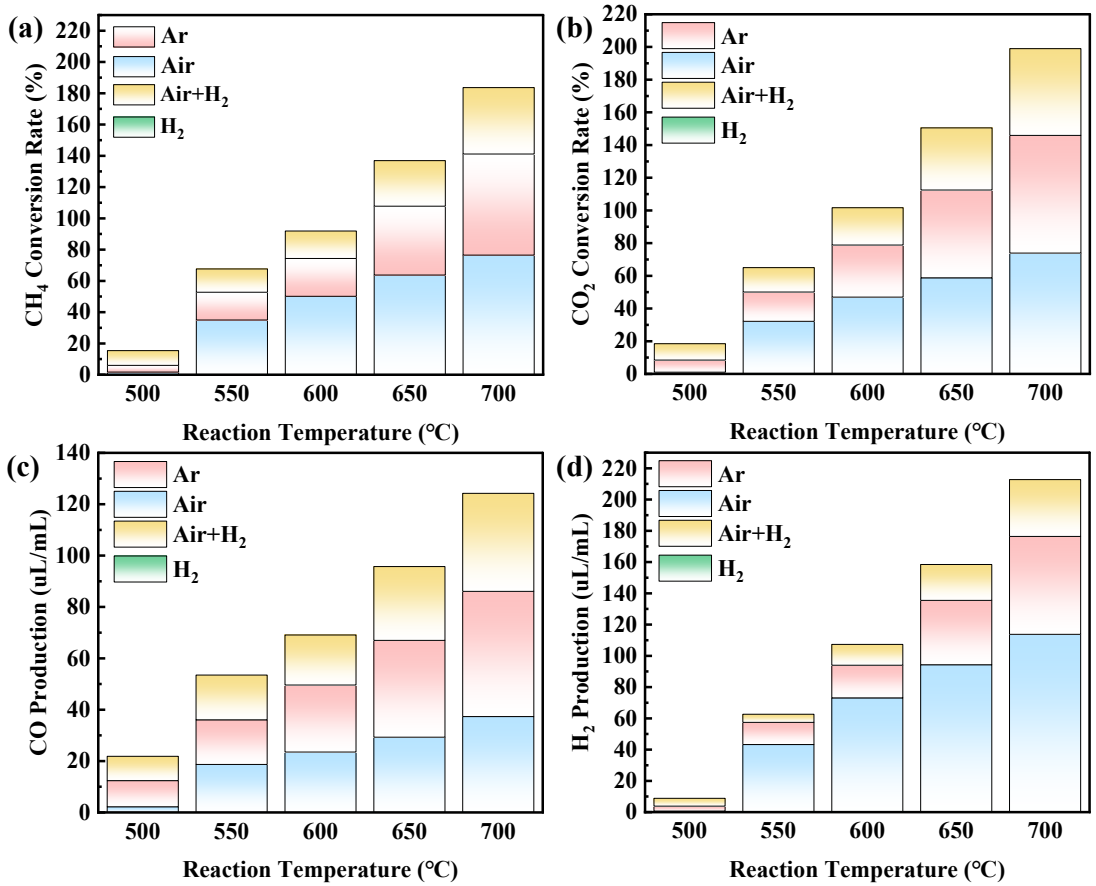

141

142 **Fig. S6** The DRM activity: (a) CH_4 conversion rate, (b) CO_2 conversion rate, (c) CO

143 production, and (d) H_2 production.

144

Table. S3 Performance comparison of developed catalysts in DRM.

Sample	Reaction temperature (°C)	Flow rate (mL min^{-1})	Quality (mg)	Ratio of H_2/CO	Ref.
NMO-Air	700	30	50	1.2	This work
$CaZr_{0.8}Ni_{0.2}O_{3-\delta}$	800	80	600	0.95	[3]
Ni-CeO_2	500	GHSV: 48000 h^{-1}		0.7	[4]
Ni_1/CoCe	800	30	100	0.95	[5]
Ni@Co_1/CeO_2	800	30	20	0.8	[6]
55Ni/CeO_2-G	700	50	100	0.8	[7]
1.2Ni-0.3Co-SiO_2	700	20	30	0.43	[8]
N3M/A	700	100	200	0.8	[9]

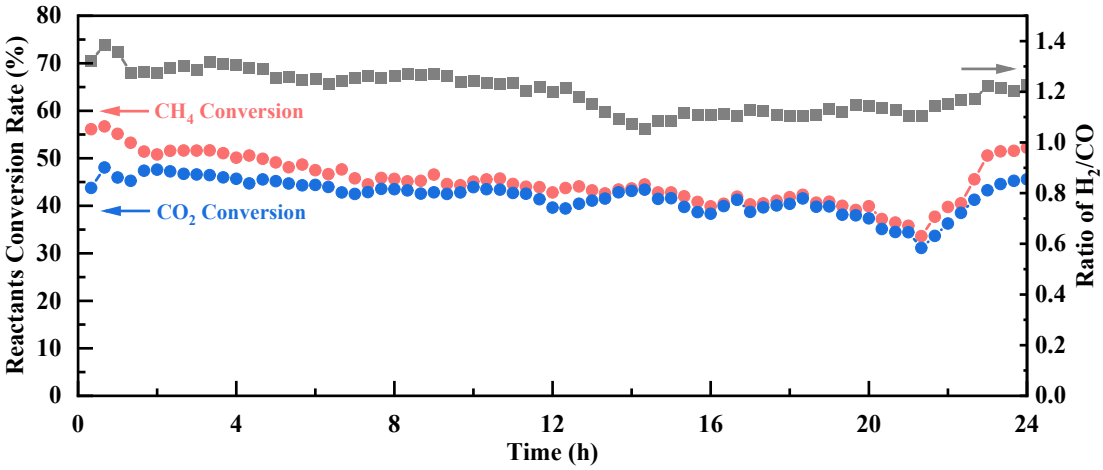

147

148 **Fig. S7** the DRM reaction stability of NMO-Air under 600 °C for 24 h. Flow rate: 30

149 30 mL min^{-1} ($CH_4/CO_2/Ar$=1/1/3), catalyst quality: 50 mg.

150

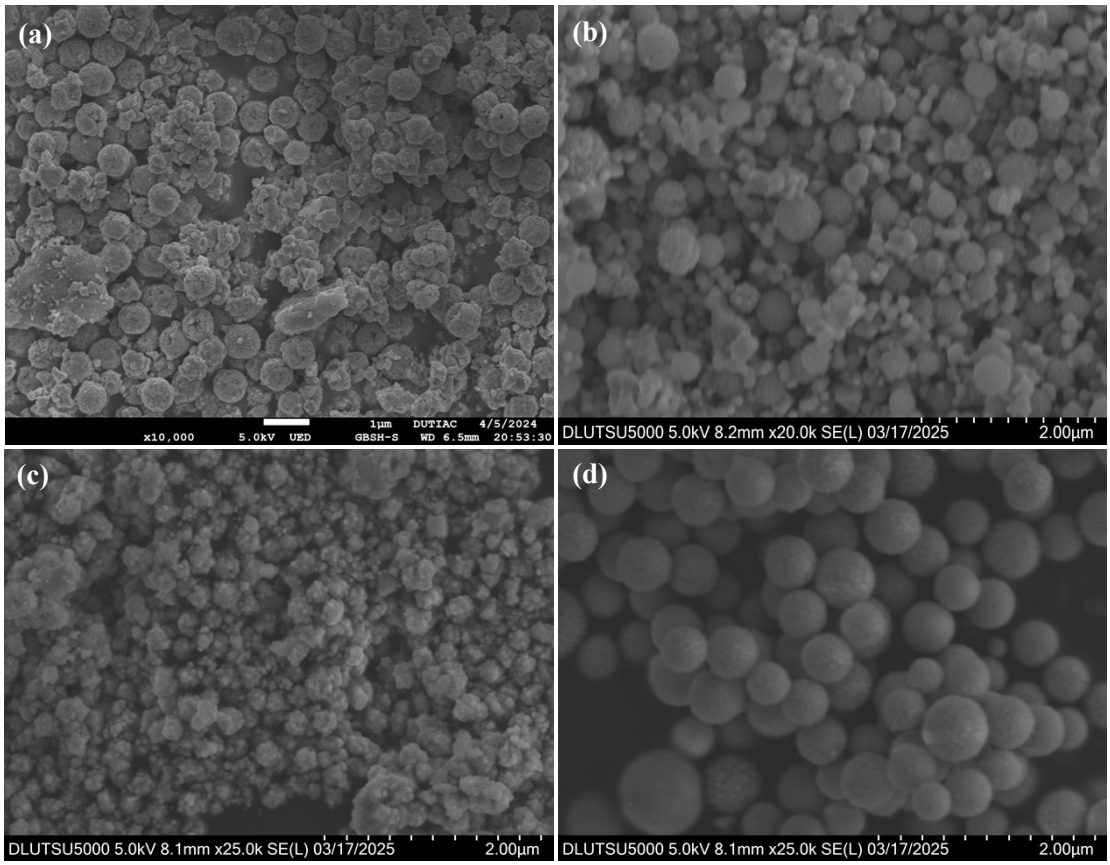

Fig. S8 The SEM images after reaction: (a) NMO-Air, (b) NMO-Ar, (c) NMO-Air+H_2, and (d) NMO-H_2.

The spherical structure of NMO-Ar exhibited partial separation after reaction, attributable to its argon-atmosphere calcination. The inert argon atmosphere provided limited chemical regulation, leading to non-uniform stress distribution and inadequate lattice stability during high-temperature treatment, which aggravated structural separation under DRM conditions. In contrast, NMO-Air+H_2 underwent more severe structural collapse, revealing that hydrogen pretreatment substantially reduces structural stability. The strong reducibility of H_2 might cause excessive reduction of metal ions, disrupting crystalline integrity and diminishing morphological stability under high-temperature reaction conditions. Although catalytically inactive, NMO-H_2

underwent surface reconstruction from rough to smooth, demonstrating that controlled atmosphere treatment can induce morphological optimization.

References

1. M. Sun, W. Li, B. Zhang, G. Cheng, B. Lan, F. Ye, Y. Zheng, X. Cheng and L. Yu, *Chem. Eng. J.*, 2018, **331**, 626-635.
2. N. Huang, Z. Qu, C. Dong, Y. Qin and X. Duan, *Appl. Catal. A Gen.*, 2018, **560**, 195-205.
3. S. Dama, S. R. Ghodke, R. Bobade, H. R. Gurav and S. Chilukuri, *Appl. Catal. B Environ.*, 2018, **224**, 146-158.
4. M. Li and A. C. van Veen, *Appl. Catal. B Environ.*, 2018, **237**, 641-648.
5. J. Wu, J. Gao, S. Lian, J. Li, K. Sun, S. Zhao, Y. D. Kim, Y. Ren, M. Zhang, Q. Liu, Z. Liu and Z. Peng, *Appl. Catal. B Environ.*, 2022, **314**, 121516.
6. E. Yang, E. Nam, Y. Jo and K. An, *Appl. Catal. B Environ.*, 2023, **339**, 123152.
7. H. Xia, C. Dang, D. Zhou and W. Cai, *Chem. Eng. J.*, 2024, **489**, 151365.
8. J. Zhang, K. Xie, Y. Jiang, M. Li, X. Tan, Y. Yang, X. Zhao, L. Wang, Y. Wang, X. Wang, Y. Zhu, H. Chen, M. Wu, H. Sun and S. Wang, *ACS Catal.*, 2023, **13**, 10855-10865.
9. D. Liang, Y. Wang, M. Chen, X. Xie, C. Li, J. Wang and L. Yuan, *Fuel*, 2022, **321**, 124032.